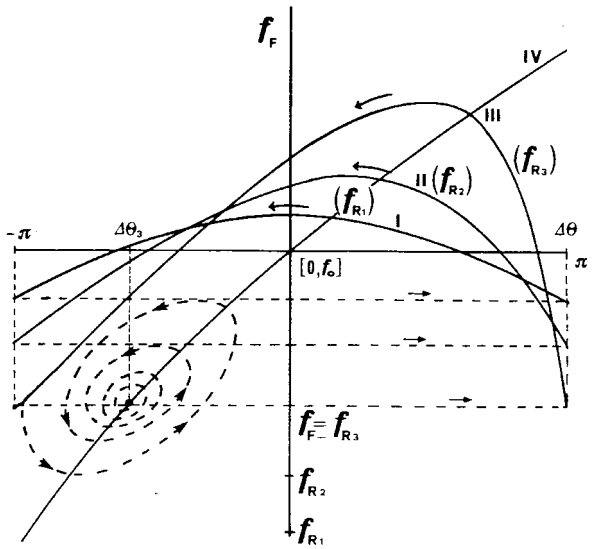

Fig. 2. Theoretical phase-plane portraits $(f_R < f_o)$.

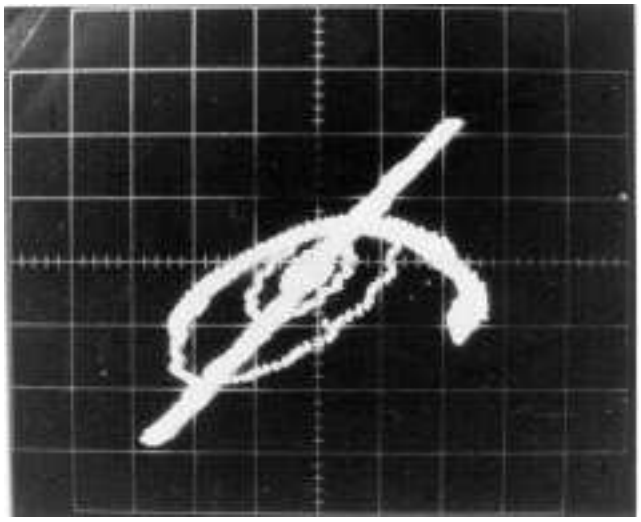

Fig. 3. Experimental oscillograph of typical $f_R < f_o$ phase-plane portraits with lock-in trajectory [axes 9.3 Hz/div. and 1.34 rad/div., $f_o = 279$ Hz, $f_R = 265$ Hz].

the motor. Unlocked operation is stable (no pull-in process), hence, given an f_R value, there is only one trajectory that represents the system and it is repeated every cycle.

Frequency variation occurring leads to the fact that, for certain f_R values, output frequency f_F may be equal at a time to f_R. The system does not lock at this moment because phase difference $\Delta\Phi$ will not (in a typical case) correspond to the f_R value. Equality of the two frequencies implies that $\Delta\Phi$ shall not be altered, hence, the trajectory curve becomes perpendicular to the $\Delta\Phi$-axis. Operating point $(\Delta\Phi - f)$ is prevented from reaching the SHPD's limiting value $(-\pi)$, and the system is entering a procedure that will drive it to lock (curve III in Fig. 2),$f_R = f_{R3})$. The detector's output shall have nearly it's maximum negative value, and the system will be driven to even smaller frequencies than f_{F-}. The hold-in range is implied here to be larger than the capture one, a fact that is certainly justified by the system's order. Feedback frequency becomes smaller than f_R, therefore, phase difference $\Delta\Phi$ is now increasing. Phase increment results soon in a frequency increment and so on. The operating point has avoided to reaching the SHPD's limit $(-\pi)$ and has entered into a trajectory that leads to a stable focus according to control system theory. The experimental oscillograph of Fig. 3 shows a typical behavior of the system developed verifying the theoretical curves of Fig. 2. The thick line at the upper part indicates that a number of cycles of unlocked operation have been recorded, before a new value of f_R (near f_O) that is entered leads the system into lock. The straight line is the system's trajectory under locked conditions (curve IV in Fig. 2). Stability of unlocked operation, as has been described, may be seen in this way, together with the effect of noise and phase jitter of an actual system. Capture range limits can also be obtained on the basis of the acquisition procedure described.

REFERENCES

[1] U. Mengali, "Acquisition behavior of generalized tracking systems in the absence of noise," *IEEE Trans. Commun.*, vol. COM-21, pp. 820–826, Aug. 1974.
[2] T. Laopoulos and C. Karybakas, "Sample and hold phase-frequency detector for phase locked loop motor speed control systems," *J. Ind. Electron.*, vol. 59, no. 2, pp. 231–234, 1985.
[3] F. M. Gardner, *Phaselock Techniques*, 2nd ed. New York: Wiley, l979.
[4] T. Laopoulos and C. Karybakas, "A phase locked motor speed control system with a sample-and-hold phase detector," *IEEE Trans. Ind. Electron.*, vol. 35, pp. 245–252, May 1988.
[5] H. L. Jou and J. C. Wu, "Fast response phase detector for a phase locked loop," *Int. J. Electron.*, vol. 78, no. 3, pp. 557–562, 1995.

A Programmable Cascaded Low-Pass Filter-Based Flux Synthesis for a Stator Flux-Oriented Vector-Controlled Induction Motor Drive

Bimal K. Bose and Nitin R. Patel

***Abstract*— The concept of programmable cascaded low-pass filter method of flux vector synthesis has been introduced in the literature [1]. In this paper, the idea will be expanded, analyzed, improved, and then applied to a stator flux oriented 100-kW electric vehicle drive. It was verified that the flux estimation works well at zero speed finite torque start-up mode and low- and high-speed field weakening regions, thus completely eliminating the need of speed sensor.**

I. INTRODUCTION

Currently, speed and flux sensorless vector control of induction motor drive is receiving wide attention in the literature. In spite of a large effort, precision synthesis of speed and flux vector signals, particularly near zero speed operation, yet remains a challenge. The stator flux-oriented vector control of induction motor drive [2] is

Manuscript received March 6, 1996; revised July 9, 1996.
The authors are with the Department of Electrical Engineering, University of Tennessee, Knoxville, TN 37996-2100 USA.
Publisher Item Identifier S 0278-0046(97)01285-9.

recently gaining more popularity because the feedback signal estimation accuracy is dependent only on the stator resistance variation which can be compensated somewhat easily. Besides, the signal voltage behind the stator resistance drop that is to be integrated for stator flux estimation is somewhat larger than that for rotor flux estimation. This signal magnitude tends to be very low near zero speed operation. If an attempt is made to integrate this signal directly near zero speed, a dc offset will appear at the output [see Fig. 3(a)]. This problem can be solved by a programmable multistage low-pass filter implemented by microcomputer/digital signal processor (DSP)-based software. For a stator flux-oriented vector-controlled electric vehicle (EV) type of drive where speed signal is not needed, this type of sensorless control becomes very attractive.

In this paper, the concept of the programmable cascaded low-pass filter method of flux estimation will be expanded, systematically analyzed, designed, verified by simulation study, and then integrated with a 100-kW drive for practical EV application.

II. Description of Cascaded Low-Pass Filter

Fig. 1(a) shows the control block diagram of a stator flux-oriented EV induction motor drive that incorporates the cascaded low-pass filter flux estimation, and Fig. 1(b) shows the details of the filter. The drive has torque and flux control in the outer loops. The flux loop is added with decoupling compensation current i_{dq} which is characteristic of stator flux-oriented control [2]. The machine terminal voltages and currents are sensed and passed through hardware low-pass filters (not shown) before A/D conversion. The hardware filters also transform the input signals into $d^s - q^s$ frame, as indicated.

The principle of the cascaded low-pass filter method of integration can be explained as follows. Since the drive has to operate in a wide frequency range (including zero speed condition), a single-stage integrator has to be designed with a very large time constant. This causes the problem of dc offset and its very slow decay, as dictated by the time constant. If, on the other hand, a single-stage integrator is resolved into a number of cascaded low-pass filters with a short time constant, the problem of dc offset decay time can be sharply attenuated. Consider a low-pass filter with transfer characteristic as

$$Y/X = 1/1 + j\tau\omega_e \tag{1}$$

where τ = time constant and ω_e = frequency. The phase lag and gain (or attenuation) of the filter at frequency ω_e can be given, respectively, as

$$\phi = \tan^{-1}(\tau\omega_e) \tag{2}$$

$$K = |Y/X| = 1/\sqrt{1 + (\tau\omega_e)^2}. \tag{3}$$

If n number of filters are cascaded, the total phase shift angle and gain are given, respectively, as

$$\phi_T = \phi_1 + \phi_2 + \cdots + \phi_n = \tan^{-1}(\tau_1\omega_e) + \tan^{-1}(\tau_2\omega_e) + \cdots + \tan^{-1}(\tau_n\omega_e) \tag{4}$$

$$K_T = K_1K_2\cdots K_n = 1/\sqrt{[1 + (\tau_1\omega_e)^2][1 + (\tau_2\omega_e)^2]\cdots[1 + (\tau_n\omega_e)^2]}. \tag{5}$$

If all the filter stages are identical, the corresponding expressions are

$$\phi_T = n\phi = n\tan^{-1}(\tau\omega_e) \tag{6}$$

$$K_T = nK = \frac{1}{\sqrt{[1 + (\tau\omega_e)^2]^n}}. \tag{7}$$

If the cascaded filter performs integration of a sinusoidal voltage, then $\phi_T = 90^\circ$ and $G \cdot K_T = 1/\omega_e$, where G = gain compensation needed for integration. Substituting these conditions in (6) and (7)

$$\tau = (1/\omega_e)\tan(90^\circ/n) \tag{8}$$

$$G = (1/\omega_e)\sqrt{[1 + \tau\omega_e)^2]^n}. \tag{9}$$

The above equations give the parameters τ and G as a function of frequency. A large number of n is desirable, but the software computation burden becomes heavy. Fig. 1(b) considers $n = 3$, and in addition, gives correction for frequency-sensitive phase shift (ϕ_h) and gain introduced by the analog hardware filter in the front end. Therefore, the correct gain and time constant expressions can be derived as

$$\tau = (1/\omega_e)\tan[(1/n)[\tan^{-1}(\tau_h\omega_e) + 90^\circ]] = f(\cdot)\omega_e \tag{10}$$

$$G = (1/\omega_e)\sqrt{[1 + (\tau\omega_e)^2]^n[1 + (\tau_h\omega_e)^2]} = g(\cdot)\omega_e \tag{11}$$

where τ_h = hardware filter time constant (0.16 ms). Note that the hardware filters can be conservatively designed without fear of phase drift and attenuation of the signals because these are compensated in the software filters. Fig. 2(a) and (b) shows the plots of τ and G as a function of ω_e according to the above equations. Note that with programmable τ and G, the phase shift and gain are equal in all the filter stages and they remain invariant with frequency. The fluxes ψ^s_{ds} and ψ^s_{qs} are further phase-shifted by angle ϕ_h to generate $\psi^{s'}_{ds}$ and $\psi^{s'}_{qs}$. These auxiliary fluxes which are at phase quadrature with the respective currents i^s_{ds} and i^s_{qs} help to generate the unit vector signals for inverse vector rotation of currents as indicated below. The remaining computations by signal computation block of Fig. 1(a) are as follows:

$$\psi_s = \sqrt{(\psi^s_{ds})^2 + (\psi^s_{qs})^2} \tag{12}$$

$$\cos\theta_e = \psi^s_{ds}/\psi_s \tag{13}$$

$$\sin\theta_e = \psi^s_{qs}/\psi_s \tag{14}$$

$$\cos\theta'_e = \psi^{s'}_{ds}/\sqrt{(\psi^{s'}_{ds})^2 + (\psi^{s'}_{qs})^2} \tag{15}$$

$$\sin\theta'_e = \psi^{s'}_{qs}/\sqrt{(\psi^{s'}_{ds})^2 + (\psi^{s'}_{qs})^2} \tag{16}$$

$$\omega_e = [(v^s_{qs} - i^s_{qs}R_s)\psi^s_{ds} - (v^s_{ds} - i^s_{ds}R_s)\psi^s_{qs}]/\psi^2_s. \tag{17}$$

Note that if the stator resistance variation is not adequately compensated, a small amount of error will be introduced in all the signals estimated above. The error in ω_e estimation will affect the accuracy of the cascaded filter.

III. Performance Evaluation

The cascaded low-pass filters were designed and studied in detail by simulation with the drive system shown in Fig. 1(a). The drive was

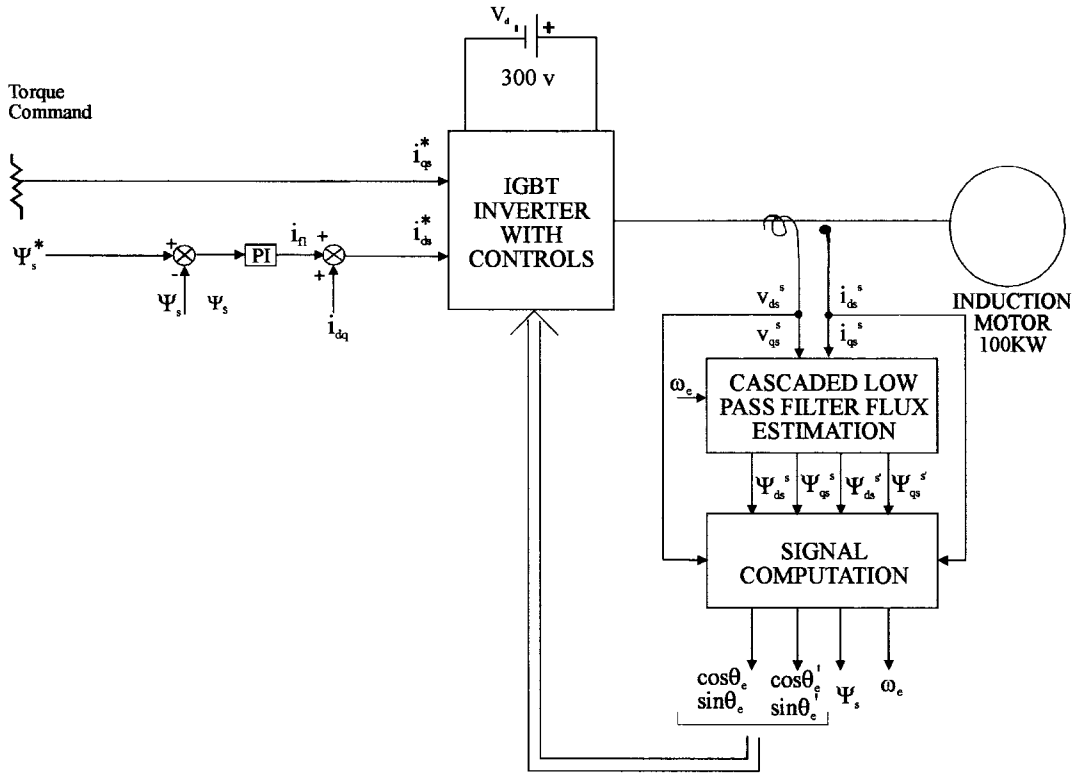

(a)

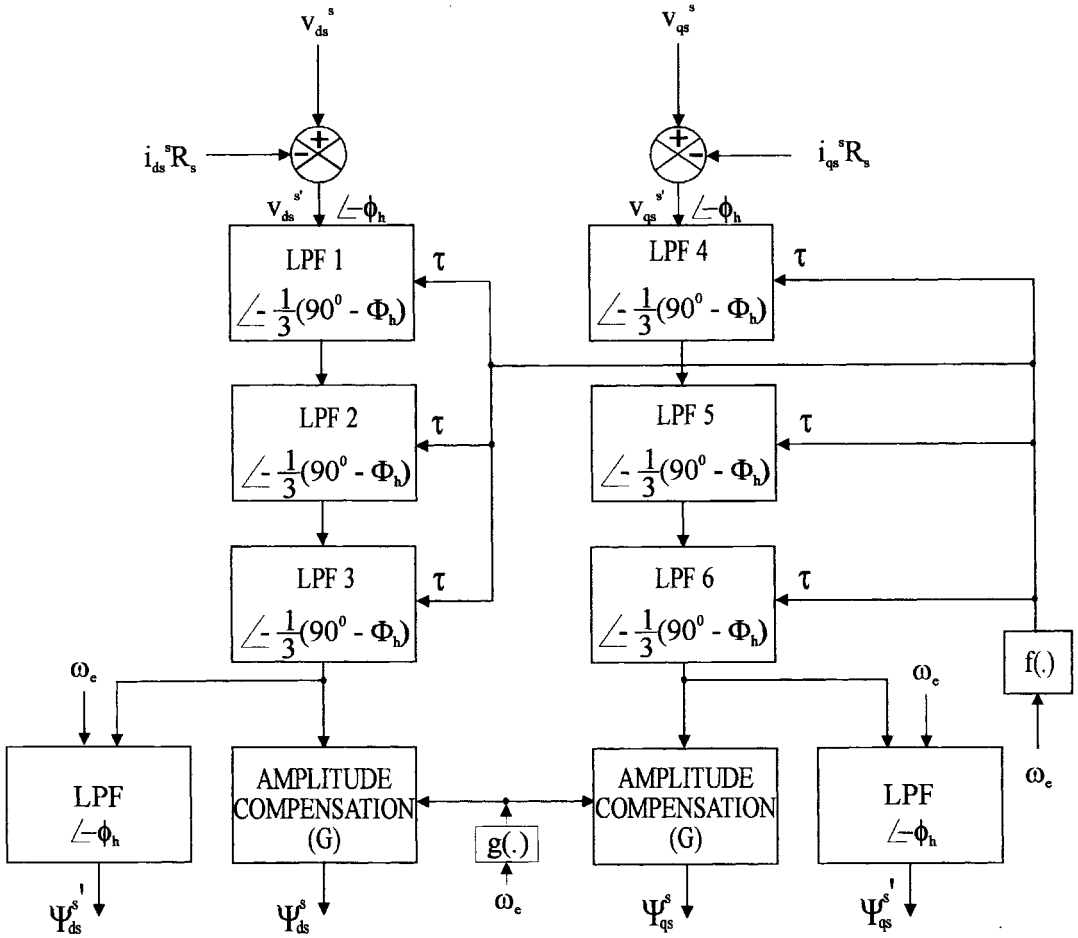

(b)

Fig. 1. (a) Control block diagram of stator flux-oriented vector control with cascaded low-pass filter-based flux estimation. (b) Cascaded low-pass filter implementation block diagram.

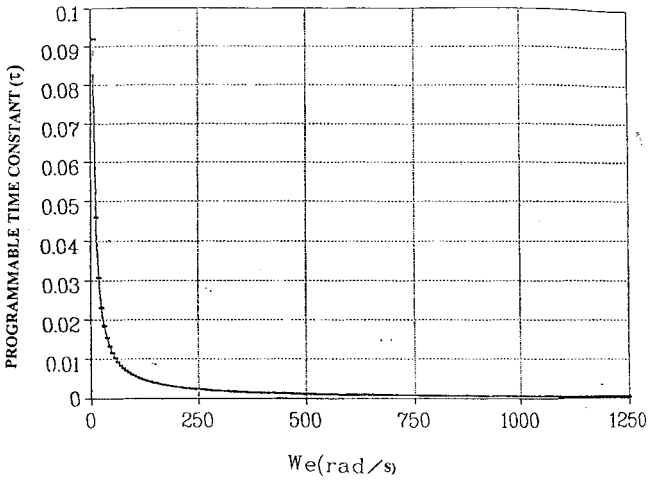

(a)

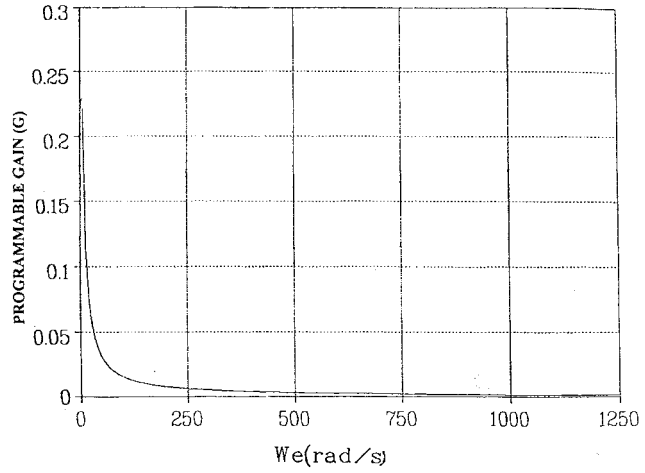

(b)

Fig. 2. Programmable time constant and gain of the filter. (a) Programmable time constant with frequency. (b) Programmable gain compensation with frequency.

initially started in stator flux-oriented indirect vector control mode [1], and with a finite torque (i.e., with finite slip frequency ω_{sl}) but zero speed, it was switched to the direct vector control mode shown in Fig. 1(a). A new start-up method in direct vector control mode has been developed which will be reported later. As the drive is switched to the direct vector control mode, the frequency (ω_e) is initialized with the slip (ω_{sl}) signal. Then, ω_e builds up automatically in a circulatory manner.

The performance of the drive with the cascaded filter was found to be excellent in wide frequency range. Fig. 3(a) shows the performance of a single-stage integrator with large and fixed time constant where the dc offset is evident. Fig. 3(b) shows performance of the cascaded filter integrator at low frequency, and Fig. 3(c) shows its transient performance. Note that the filter performance depends on a reasonably accurate computation of ω_e signal which tends to be difficult at very low frequency (fraction of a hertz). The control system is now being implemented on a TMS320C30-based DSP for 100-kW EV drive application. The experimental performance of the drive along with all the control features will later be presented in a full paper.

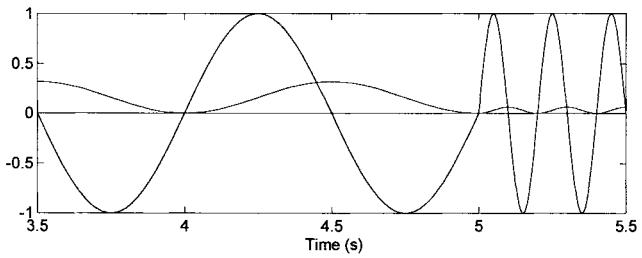

(a)

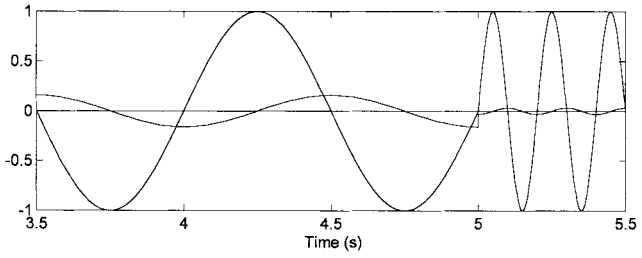

(b)

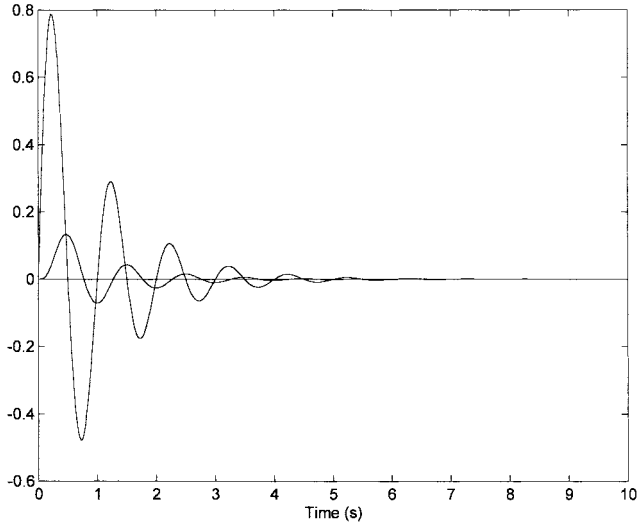

(c)

Fig. 3. Flux estimation performance. (a) Single-stage integrator (with fixed time constant). (b) Cascaded low-pass filter at steady state. (c) Cascaded low-pass filter at transient condition.

IV. Conclusion

A software programmable cascaded low-pass filter has been investigated for flux vector synthesis of a stator flux-oriented direct vector-controlled induction motor drive. The integrator has been studied in detail with the drive system in wide frequency range by simulation and performance was found to be excellent.

References

[1] B. K. Bose, M. G. Simoes, D. R. Crecelius, K. Rajashekara, and R. Martin, "Speed sensorless hybrid vector controlled induction motor drive," in *Conf. Rec. IEEE-IAS Annu. Mtg.*, 1995, pp. 137–143.

[2] X. Xu, R. W. De Donker, and D. W. Novotny, "A stator flux oriented induction motor drive," in *Conf. Rec. IEEE-PESC*, 1988, pp. 870–876.

[3] B. K. Bose, Ed., *Power Electronics and Variable Frequency Drives*. Piscataway, NJ: IEEE, 1997.